Modification of the Crystallization Kinetics of a Mixed Bath of Alkanes in the Presence of Coil-Crystalline Block Copolymer Micelles

D. Buzza, T. Mcleish

J. Phys. II France 7 (1997) 1379–1392 OCTOBER 1997, PAGE 1379

Modification of the Crystallization Kinetics of a Mixed Bath of Alkanes in the Presence of Coil-Crystalline Block Copolymer Micelles

D.M.A. Buzza (*) and T.C.B. McLeish

I.R.C. in Polymer Science and Technology, Leeds University, Leeds LS2 9JT, UK

(Received 20 September 1996, revised 16 April 1997, accepted 23 June 1997)

PACS.61.25.Hq – Macromolecular and polymer solutions; polymer melts; swelling
PACS.82.65.Dp – Thermodynamics of surfaces and interfaces

Abstract. — Recent Neutron Scattering experiments by Richter *et al.* [1] show that the presence of coil-crystalline block copolymer (PE-PEP) micelles in a mixed alkane bath suppresses the crystallization out of solution of the long alkane component at low temperatures. Motivated by these experiments, we study theoretically the thermodynamics and kinetics of lamellar coil-crystalline block copolymer micelles in a bimodal solvent to better understand the factors determining the anti-precipitation action of coil-crystalline block copolymers. We assume an Alexander-de Gennes brush model for the strongly stretched corona chains and explicitly account for the polydispersity of the solvent chains. For the thermodynamic distribution of solvent chains in the corona, we find a predominance of short solvent chains to long solvent chains in the corona phase compared to the solvent bath, both with and without nematic interactions in the corona phase. We also calculate the rate of crystallization of the long solvent chains onto the micellar crystal core and find that the rate is sensitive to both brush and core parameters. In particular, we predict that to maximize the rate, both $E_{\mathrm{fold}}/kTN_{\mathrm{A}}$ and χ_{n} need to be made as small as possible, where E_{fold} is the folding energy of the crystal core chains, N_{A} the number of statistical segments of the solvated corona chains and χ_{n} parameterises the strength of nematic interactions in the micellar corona. This leads to the surprising result that for fixed E_{fold}, the rate of crystallization is increased when we increase the molecular weight of the corona blocks.

1. Introduction

Block Copolymers (BCPs) form many interesting structures due to their amphiphilic nature, *i.e.* the fact that two or more different chemistries are covalently bonded in the same molecule. For example when a diblock copolymer is added to a solvent for which only one component is soluble (*i.e.* a selective solvent), the BCPs form micellar aggregates where the soluble parts form an outer corona to shield the insoluble parts from energetically unfavourable contacts with the solvent. In the case where the insoluble block is also crystallizable (*i.e.* a coil-crystalline BCP) the core of the BCP micelle will be crystalline.

Recent experiments by Richter *et al.* [1] on the crystallization behaviour of a mixed alkane bath have yielded an interesting result. The specific system studied consisted of a small amount

(*) Author for correspondence (e-mail: phydmb@phys-irc.novell.leeds.ac.uk)

of a higher molecular weight alkane (*e.g.* $C_{36}H_{74}$, or C_{36} for short) in a bath of decane (*i.e.* $C_{10}H_{22}$). They found that the addition of the block copolymer PE-PEP significantly lowered the temperature at which the high molecular weight alkane crystallizes out of solution. It is known that PE-PEP is a coil-crystalline BCP (the PE block is crystallizable) and that above its Critical Micellar Concentration (C.M.C.), it forms lamellar micelles in decane with a crystalline PE core [2,3] (see Sect. 2). Because of this, it was initially thought that the lowering of the precipitation temperature of the long alkane was due to the co-crystallization of these chains within the crystalline PE core. However Small Angle Neutron Scattering (SANS) has shown that the PEP corona rather than PE crystal core of the micelle is swollen when the temperature is lowered below the normal crystallization temperature of the long alkane in decane [1]. By measuring the surface to volume ratio of the crystalline regions in solution via SANS, Richter *et al.* were able to further conclude that the long alkane was crystallizing onto the surface of the crystalline PE core. Since it is well known that the crystallization of alkanes in solution proceeds *via* nucleation (*e.g.* Refs. [4]), Richter *et al.* have suggested that the suppression of long alkane precipitation is due to the PE crystal surfaces of the PE-PEP micelles acting as alternative nucleation sites for the crystallization of the long alkanes. This implicitly sets up a competition between normal crystallizaton processes in the alkane bath and crystallization onto the PE crystal core. Given that we are considering a kinetic process (i.e. nucleation), the actual kinetic path that the system adopts is the fastest pathway. The aim of this paper therefore is to calculate theoretically the rate of crystallization onto the crystal core in order to better understand the factors determining the effectiveness of coil- crystalline BCPs in suppressing long alkane precipitation.

Although there have been previous studies of the crystallization of PE or alkanes onto crystal lamellae (*e.g.* Ref. [5]), there are at least two novel features in the experimental study of Richter *et al.* The first is the presence of a solvated polymer layer (the corona) on top of the crystal substrate. We will show in Section 4 that this feature modifies the kinetics of crystallization compared to the case of a "bare" crystal substrate. This means that the polymer corona plays two distinct roles: the kinetically neutral role of keeping the crystal cores in solution and separating the crystal cores from each other so that the crystal regions are finely dispersed and do not precipitate out of solution; in addition it also plays the kinetically active role of modifying the crystallization rate onto the PE core surface. The second novel feature is that crystallization occurs from a mixed bath system rather than a single component system. Our theoretical calculation will take into account both features in the experiments. In Section 2, we first calculate the thermodynamic distribution of short and long chains in the polymer corona compared to that in the bath. Section 3 considers the effect on this thermodynamic distribution when we include nematic interactions in the corona phase. The motivation for this is the evidence that a pre-transitional nematic effect can be important in alkanes [6, 7], and is therefore a candidate for favourable interactions between the alkanes and the corona. Due to the presence of an energy barrier at the phase boundary between the crystal core and alkane bath, the crystallization of long alkanes onto the PE core is an activated process. Because of this, the results from Sections 2 and 3 contribute to Section 4, where we calculate the crystallization rate of long chains onto the PE core surface. Section 5 is our conclusions section.

2. Thermodynamic Distribution of Solvent Chains in the Corona

In this section, we calculate the thermodynamic distribution of solvent (alkane) chains in the corona phase. This distribution applies to the corona phase of Richter *et al.* system above the crystallization temperature of the long alkane chains. In order to proceed, we need more

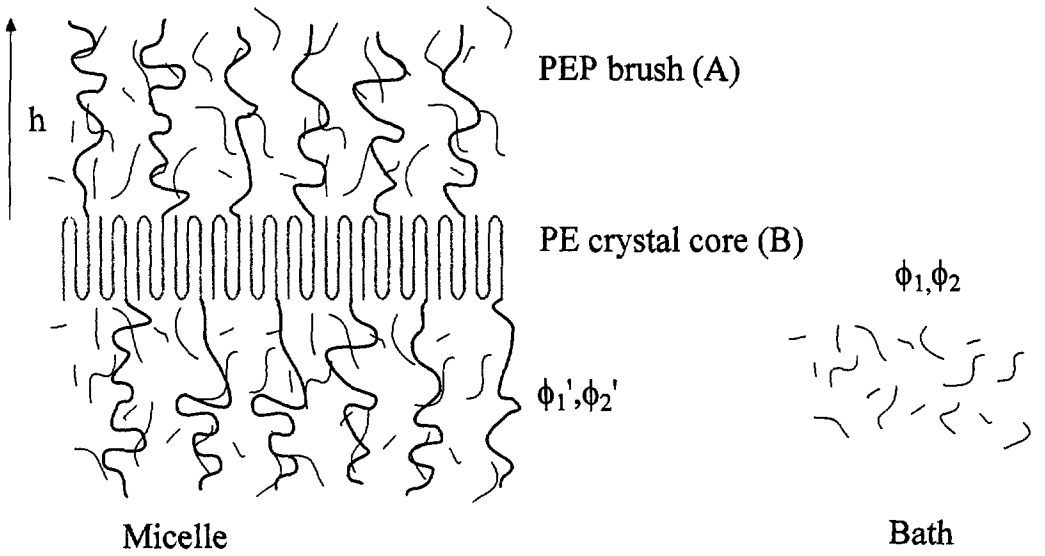

Fig. 1. — A-B coil-crystalline block copolymer micelle in a solvent bath containing short (N_1 links) and long (N_2 links) solvent chains. The B core is crystalline, while the solvated A blocks from a highly stretched polymer brush.

information on micellar structure. This has been elucidated by Richter and coworkers using neutron scattering [2,3]. They have shown that the PEP-PE block copolymers form lamellar micelles with crystalline PE cores while the PEP blocks emanate from either side of the core to form the corona. Note that the driving force for micellization in this case is the crystallization energy of the PE chains rather than the incompatibility parameter χ between PE and the solvent. Also, for the molecular weights used (around 5k to 10k for each arm), the PEP blocks were found to be highly stretched to many times their radius of gyration (about 3 to 5 times), *i.e.* they form a polymer brush.

Based on this information, in Figure 1 we show an A-B micelle in a solvent bath. The B blocks are crystalline with the chains folding back and forth as shown while the soluble A blocks are highly stretched to height h. As in Richter's experimental system, we shall consider a bimodal solvent bath containing a short chain component (length L_1), and a long chain component (length L_2). If a is the statistical segment length for the solvent chains, then the number of statistical links of the short and long chains is given by $N_1(\equiv L_1/a)$ and $N_2(\equiv L_2/a)$ respectively ($N_2 > N_1$). The volume fraction of the short and long components is ϕ_1, ϕ_2 respectively in the bath and ϕ_1', ϕ_2' respectively in the brush.

In order to find ϕ_1', ϕ_2', we require the free energy of the brush phase and the bath. We will assume the simplest model for the brush, due to Alexander and de Gennes [8,9]. A more sophisticated (and accurate) self-consistent field method for polymer brushes exists [10] and may be employed if a more refined version of the present calculation is required. The Alexander-de Gennes model assumes a step function of height h for the monomer concentration profile (so that ϕ_1', ϕ_2' are independent of the distance z from core brush interface) and all the chain ends are at $z = h$. Working within the framework of a Flory Huggins type lattice model (lattice cell length a), we can define free energies per site for the system. For the brush phase this is

given by

$$\frac{F_{\text{site}}^{\text{brush}}}{kT} = \frac{1}{2}\frac{(1-\phi_1'-\phi_2')}{N_A}\frac{h^2}{N_A a^2} + \frac{\phi_1'}{N_1}\ \ln\ \phi_1' + \frac{\phi_2'}{N_2}\ \ln\ \phi_2' + \frac{E_{\text{fold}}}{kT}\frac{a}{h} \tag{1}$$

where N_A is the number of statistical segments of the A (brush) chains and E_{fold} is the folding energy of the B (core) chains. The first term on the right hand side is the stretching energy (per site) of the brush chains; this term penalises strong stretching of the brush. The second and third terms are the translational entropy of short and long chains respectively in the brush (the Flory interaction parameter between solvent and brush chains is assumed to be zero). These terms contribute an effective interaction which tends to swell the brush. The reason we have adopted the Flory-Huggins free energy for solvent chains instead of the excluded volume interaction between brush chains [10] is to explicitly account for the different lengths of solvent chains. The last term is the interfacial energy of the crystal core/brush interface which tends to reduce the interfacial area. Note that the main contributon to interfacial energy (or surface tension) comes from the folding energy of core chains rather than the incompatibility between the core and solvent, as is the case when the core is amorphous. Although the PE core is crystalline, the chains within the crystal lattice are fairly mobile [11] so that the number of folds per chain is not fixed, *i.e.* the cystal core is a "thermodynamic" crystal [12]. This means that unlike in the case of end grafted polymer brushes, the surface area per chain Σ is not a quenched variable in this system. Because of this, there are three independent variables in the brush free energy, ϕ_1', ϕ_2' and Σ or alternatively ϕ_1', ϕ_2' and h, since the Σ and h are related via the volume per chain by

$$\Sigma = \frac{N_A a^3}{h(1-\varphi_1'-\varphi_2')}\,. \tag{2}$$

In this paper we will use ϕ_1', ϕ_2' and h as our independent variables in the problem. Vilgis and Halperin [12] have also considered the thermodynamic properties of lamellar coil-crystalline BCP micelles (as shown in Fig. 1) using a scaling theory. Our treatment is essentially the same as theirs except for the fact that we have explicitly accounted for polydispersity of the solvent (alkane) molecules, since the main focus of this paper is the distribution of solvent chains within the brush (corona) phase.

The free energy in the bath is just given by the translational entropy of the solvent chains, *i.e.*

$$\frac{F_{\text{site}}^{\text{bath}}}{kT} = \frac{\phi_1}{N_1}\ \ln\ \phi_1 + \frac{\phi_2}{N_2}\ln\phi_2. \tag{3}$$

The chemical potential (per monomer) of species i is given in terms of F_{site} and volume fractions of different species by [13]

$$\mu_i = F_{\text{site}} + \frac{\partial F_{\text{site}}}{\partial \phi_i} - \sum_j \phi_j \frac{\partial F_{\text{site}}}{\partial \phi_j} \tag{4}$$

where the summation is over all different species. To find the equilibrium brush height h and ϕ_1', ϕ_2', we minimize F_{brush} with respect to h and balance the chemical potentials of species 1 and 2 in both the brush and the bath. From equations (1), (3) and (4) we then obtain the following set of simultaneous equations

$$\frac{h}{a} = N_A^{2/3}\left(\frac{E_{\text{fold}}}{kT}\right)^{1/3}(1-\phi_1'-\phi_2')^{-1/3} \tag{5}$$

$$\left(\frac{\phi_1'}{\phi_1}\right)^{1/N_1} = \left(\frac{\phi_2'}{\phi_2}\right)^{1/N_2} \tag{6}$$

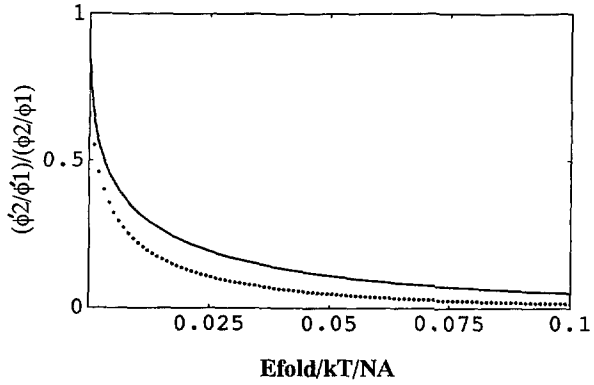

Fig. 2. — $(\phi_2'/\phi_1')/(\phi_2/\phi_1)$ *vs.* $E_{\rm fold}/N_{\rm A}kT$ for $E_{\rm fold}/kT = 7$, $N_1 = 2$, $N_2 = 8$, $\phi_1 = 0.98$, $\phi_2 = 0.02$; solid line without nematic interaction ($\chi_{\rm n} = 0$); dotted line for maximum nematic interaction ($\chi_{\rm n} = 1$).

$$\frac{1}{N_1}\ln\frac{\phi_1'}{\phi_1} = \left(\frac{\phi_1'}{N_1}+\frac{\phi_2'}{N_2}\right) - \left(\frac{\phi_1}{N_1}+\frac{\phi_2}{N_2}\right) - \frac{a}{h}\frac{E_{\rm fold}}{kT}. \tag{7}$$

By substituting equations (5) and (6) into (7), we can solve for ϕ_1' numerically, and hence obtain ϕ_2' and h as well.

In Figure 2 we plot ϕ_2'/ϕ_1' (normalized to the ratio in the bath) against $E_{\rm fold}/KTN_{\rm A}$ (solid line), since ϕ_2'/ϕ_1' depends on $E_{\rm fold}$ and $N_{\rm A}$ only through this combination. The other parameters are fixed at typical values for experimental system studied: $E_{\rm fold}/kT = 7$, $N_1 = 2$, $N_2 = 8$, $\phi_1 = 0.98$, $\phi_2 = 0.02$. Clearly, $\phi_2'/\phi_1 < \phi_2/\phi_1$ for all values of $E_{\rm fold}/kTN_{\rm A}$. Note that $E_{\rm fold}/kTN_{\rm A}$ expresses the competition between the elastic term ($N_{\rm A}$) and the surface tension term ($E_{\rm fold}/kT$) in the free energy. The elastic term reduces the stretching of the brush chains thereby increasing the surface area per brush chain and diluting the brush chain concentration in the brush phase. Conversely, the surface tension term decreases the surface area per chain and increases the brush chain concentration. Decreasing $E_{\rm fold}/kTN_{\rm A}$ therefore causes the brush phase to resemble the solvent bath more. This is clearly seen in Figure 2 by the fact that as $E_{\rm fold}/kTN_{\rm A} \to 0$, ϕ_2'/ϕ_1', approaches the long to short chain ratio in the bath. This fact is confirmed more explicitly in Figure 3 (solid line), where we see that the surface area per brush Σ is a monotonically decreasing function of $E_{\rm fold}/kTN_{\rm A}$. Using de Gennes' scaling language [9], when we decrease $E_{\rm fold}/kTN_{\rm A}$, the "blob" size of the brush chains increases and conversely the brush concentration goes down. In Figure 4, we plot ϕ_2'/ϕ_1' (normalized) against N_2/N_1 (solid line), with $E_{\rm fold}/kT = 7$, $N_1 = 2$, $N_{\rm A} = 100$, $\phi_1 = 0.98$, $\phi_1 = 0.98$, $\phi_2 = 0.02$. Again, we see that $\phi_2'/\phi_1' < \phi_2/\phi_1$ for all values of N_2/N_1. Note that ϕ_2'/ϕ_1' (normalized) $= 1$ for $N_2/N_1 = 1$ as required.

Thus for all experimental parameters our system, our calculation predicts that there is a predominance of short chains within in the brush phase. In fact, we can come to the same conclusion using equation (6) alone without having to solve for ϕ_1', ϕ_2' explicitly. The argument is as follows. Rearranging equation (6), we have

$$\phi_2' = \phi_2\left(\frac{\phi_1'}{\phi_1}\right)^{N_2/N_1} = \phi_2\left(\frac{\phi_1'}{\phi_1}\right)^{\alpha} \tag{8}$$

where $\alpha \equiv N_2/N_1 > 1$. Now because of the presence of A blocks in the brush phase, we must have $\phi_1' + \phi_2' < \phi_1 + \phi_2 = 1$. This together with equation (8) implies that $\phi_1'/\phi_1 < 1$.

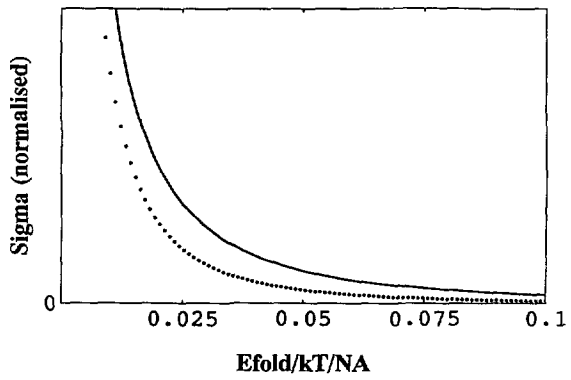

Fig. 3. — Normalized area per brush chain Σ/a^2 *vs.* $E_{\text{fold}}/N_{\text{A}}kT$ for $E_{\text{fold}}/kT = 7$, $N_1 = 2$, $N_2 = 8$, $\phi_1 = 0.98$, $\phi_2 = 0.02$; solid line without nematic interaction ($\chi_{\text{n}} = 0$); dotted line for maximum nematic interaction ($\chi_{\text{n}} = 1$).

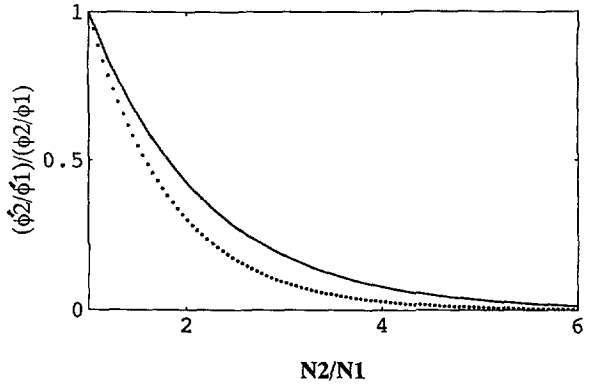

Fig. 4. — $(\phi_2'/\phi_1')/(\phi_2/\phi_1)$ *vs.* N_2/N_1 for $E_{\text{fold}}/kT = 7$, $N_1 = 2$, $N_{\text{A}} = 100$, $\phi_1 = 0.98$; $\phi_2 = 0.02$ solid line without nematic interaction ($\chi_{\text{n}} = 0$); dotted line for maximum nematic interaction ($\chi_{\text{n}} = 1$).

Now from equation (8), we have

$$\frac{\phi_2'}{\phi_1'} = \frac{\phi_2}{\phi_1}\left(\frac{\phi_1'}{\phi_1}\right)^{\alpha-1} \tag{9}$$

Since $\alpha - 1 > 0$ and $\phi_1'/\phi_1 < 1$, we arrive at the same conclusion as before, *i.e.* $\phi_2'/\phi_1' < \phi_2/\phi_1$. This is what we would expect intuitively, since short chains should enter the restricted enviroment of the brush more readily compared to long chains.

3. Effect of Nematic Interactions in the Corona on Thermodynamic Distribution

In this section, we calculate the thermodynamic distribution of solvent chains when nematic interactions are included in the brush phase free energy. The motivation for doing this is that there is both experimental (*e.g.* [6]) and theoretical (*e.g.* [7]) evidence pointing to the presence of nematic interactions in flexible polymer chains even though one does not normally associate

nematic behavior to such chains. If we accept the possibility of nematic interactions in our system, the strong uniaxial stretching of brush chains then provides a very natural driving force for nematic ordering of solvent chains within the brush phase, and so is a candidate for significant modification of the results of the last section.

To admit the possibilty of nematic interactions in the brush phase, we include the orientational free energy into the expression for the brush free energy in equation (1). We shall use expressions due to Khoklov and Semenov [14, 15] (and further clarified in [16]) for persistent semi-flexible chains in a nematic field. These are

$$\frac{F^{\text{brush}}_{\text{orient/site}}}{kT} = F_{\text{interaction}}(S) + F_{\text{entropy}}(S) + \left(\frac{\phi_1'}{N_1} + \frac{\phi_2'}{N_2}\right) F_{\text{end}}(S) \tag{10}$$

where S is the order parameter of chains in the brush phase. It is related to $f(\Omega)$, the orientational distribution function of chains in the brush phase by

$$S = \int P_2(\cos\theta) f(\Omega) \mathrm{d}\Omega$$

where $P_2(\cos\theta)$ is the second order Legendre Polynomial. Following Onsager [17], for $f(\underline{n})$ Khokhlov and Semenov use the trial function

$$f(\theta) = \left(\frac{\alpha}{4\pi \sinh\alpha}\right) \cosh(\alpha \cos\theta)$$

where θ is the angle a given segment makes with the nematic director $\underline{n}$ and α is a parameter that measures the degree of nematic order ($\alpha = 0$ in the isotropic state, $\alpha \gg 1$ for a highly ordered state). The first term on the rhs of equation (10) [16, 17]

$$F_{\text{interaction}}(S) = \frac{\pi}{4}\frac{D}{a}\left(\frac{2I_2(2\alpha)}{(\sinh\alpha)^2} - 1\right) \tag{11}$$

is the free energy per site from the orientational excluded volume interaction where D is diameter of a statistical segment ($D \sim 2$ Å and $a \sim 8$ Å so we choose $D/a = 0.25$) and $I_2(2\alpha)$ a Bessel function. (The -1 in brackets ensures that $F_{\text{interaction}} = 0$ in the isotropic state $\alpha = 0$.) The second and third terms on the right hand side of equation (10) come from the free energy per site due to orientational entropy. The leading order term

$$F_{\text{entropy}}(S) = \frac{1}{8}\int \mathrm{d}\Omega \frac{1}{f}\left(\frac{\partial f}{\partial \theta}\right)^2 \tag{12}$$

is equivalent to the orientational entropy of an infinite persistent semi-flexible chain, while the third term is the leading order correction to the orientational entropy due to the presence of ends. In equation (10)

$$F_{\text{end}}(S) = -2 \ln\left[\int \sqrt{f(\underline{n})}\mathrm{d}\Omega\right] + ln\ 4\pi \tag{13}$$

(the $\ln 4\pi$ ensures $F_{\text{end}} = 0$ in the isotropic state), while the prefactor in brackets converts F_{end} from end correction per chain to the end correction per site as required. Note that F_{end} is always positive [15], indicating that the presence of ends is always energetically unfavourable. We have included the leading order correction to the orientational entropy because, as can be seen in equation (10), the correction is different for short and long solvent chains. The use of equations (12), (13) for the orientational entropy is strictly speaking only accurate for chains

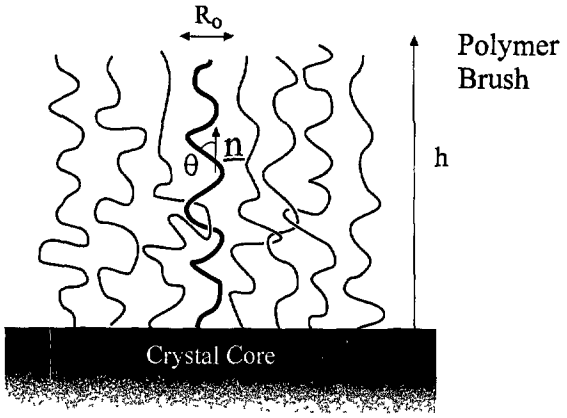

Fig. 5. — Nematic order of a monomer in a polymer brush due to strong stretching in direction $\underline{n}$ (size h). Lateral fluctuations are of the order the radius of gyration R_0 while θ is the angle between the monomer segment and the director $\underline{n}$.

where $L/a \gg 1$. We have however performed our calculation using interpolation formulas (*e.g.* Ref. [18]) which should be approximately correct over the whole range of L/a and found that equations (12), (13) give answers accurate to within 2−3% even for chain lengths $L/a \sim 1$.

To complete the specification of the problem, we need to relate the order parameter S in the brush phase to the brush height h. Refering to Figure 5, we see that the order parameter of a brush chain segment at monomer level is related to the overall stretching of the chain by (see for example Ref. [19])

$$\begin{aligned} S_{\text{brush}} &\equiv \langle P_2(\cos\theta)\rangle \\ &= \frac{1}{2}\frac{2R_z^2 - R_x^2 - R_y^2}{N_A^2 a^2} \\ &= \frac{1}{N_A}\left(\left(\frac{h}{R_0}\right)^2 - 1\right) \end{aligned} \tag{14}$$

where θ is the angle made by the monomer to the direction of stretching (z direction), and R_x, R_y and R_z are dimensions of the chain in the x, y and z directions respectively. We have also used the relation $R_x^2 = R_y^2 = R_0^2 \equiv N_A a^2$ going from the second to the third line, since the horizontal fluctuations should be of the order of the radius of gyration [9]. We now make the assumption that the order parameter of the solvent chains S_{solvent} is linearly proportional to S_{brush}, *i.e.*

$$S_{\text{solvent}} = \chi_n S_{\text{brush}} \tag{15}$$

where we define χ_n as the "nematic susceptibility", analogous to magnetic susceptibility in magnetic systems. This condition should be satisfied since we are dealing with small order parameters here (using Eq.(14), $S_{\text{brush}} \sim 0.15$ for the experimental system studied) and should therefore be far away from phase separation between solvent and brush chains [20]. The nematic susceptibilty χ_n parameterises the strength of nematic interaction between brush and solvent chains. If $\chi_n = 0$ (no nematic interation), we recover the results from Section 2. If $\chi_n = 1$, we have perfect nematic interaction. Here, we shall assume $\chi_n = 1$ to illustrate the effect of nematic interations on the solvent distribution. We expect the true solvent distribution to be

in between the results of the previous section ($\chi_n = 0$) and this section ($\chi_n = 1$). Of course, χ_n can also be left as a free parameter of our theory.

Adding the orientational free energy (Eq. (10)) to the original brush free energy (Eq. (1)), we obtain the following simultaneous equations by balancing chemical potentials and minimizing the free energy with respect to h as before:

$$\frac{h}{a} = N_A^{2/3} \left(\frac{E_{fold}}{kT}\right)^{1/3} (1 - \phi_1' - \phi_2' + g(\phi_1', \phi_2', S))^{1/3} \tag{16}$$

$$\left(\frac{\phi_2'}{\phi_2} \exp(F_{end})\right)^{1/N_2} = \left(\frac{\phi_1'}{\phi_1} \exp(F_{end})\right)^{1/N_1} \tag{17}$$

$$\frac{1}{N_1} \ln \frac{\phi_1'}{\phi_1} + \frac{F_{end}}{N_1} = \left(\frac{\phi_1'}{N_1} + \frac{\phi_2'}{N_2}\right) - \left(\frac{\phi_1}{N_1} + \frac{\phi_2}{N_2}\right) - \frac{a}{h} \frac{E_{fold}}{kT} - F_{interaction}(S) - F_{entropy}(S) \tag{18}$$

where

$$g(\phi_1', \phi_2', S) = 2 \left(\frac{\partial F_{interaction}}{\partial S} + \frac{\partial F_{entropy}}{\partial S} + \left(\frac{\phi_1'}{N_1} + \frac{\phi_2'}{N_2}\right) \frac{\partial F_{end}}{\partial S}\right). \tag{19}$$

Clearly, this set of equations is more complicated than the previous set (Eqs. (5)-(7)). However we can solve these equations self consistently, remembering that S is related to h *via* equation (14).

In Figure 2 we plot ϕ_2'/ϕ_1' (normalized) against $E_{fold}/kT = 7$ for $\chi_n = 1$ (dotted line) together with results from Section 2 (solid line). We have used the same experimental parameters for both solid and dotted lines, *i.e.* $E_{fold}/kT = 7$, $N_1 = 2$, $N_2 = 8$, $N_2 = 8$, $\phi_1 = 0.98$, $\phi_2 = 0.02$. Clearly, including nematic interactions does not change the distribution qualitatively, *i.e.* ϕ_2'/ϕ_1' is a monotonically decreasing function of E_{fold}/kTN_A, $\phi_2'/\phi_1' \to \phi_2/\phi_1$ in the limit $E_{fold}/kTN_A \to 0$ while ϕ_2'/ϕ_1' becomes very small in the opposite limit of large E_{fold}/kTN_A. Also from Figure 3 (dotted line), we see that when we include nematic interactions in the brush, the area per brush decreases with increasing E_{fold}/kTN_A, the same as in the absence of nematic interactions (solid line). However, quantitatively ϕ_2'/ϕ_1' is lower when we include nematic interactions. As we have already said, we expect the true solvent distribution to be in between the solid line and the dotted line. This fact will be true in all our following results where we compare the cases of $\chi_n = 0$ and $\chi_n = 1$.

In Figure 4, ϕ_2'/ϕ_1' (normalized) is plotted against N_2/N_1 for $\chi_n = 1$ (dots) together with results from Section 2 (solid line). The other system parameters are $E_{fold}/kT = 7$, $N_1 = 2$, $N_A = 100$, $\phi_1 = 0.98$, $\phi_2 = 0.02$. Again including nematic interactions gives us the same qualitative conclusions as in the absence of namtic interactions except ϕ_2'/ϕ_1' is lower.

From our calculations in Sections 2 and 3 we see that thermodynamics always predicts that short chains predominate over long chains in the brush phase compared with the bath, *i.e.* $\phi_2'/\phi_1' < \phi_2/\phi_1$ for all system parameters. We therefore conclude from this that the swelling of the brush by long alkane chains observed by Richter *et al.* is not a thermodynamic effect. This further confirms the suggestion of Richter *et al.* that the observed phenomenon is kinetic in origin (*i.e.* nucleation).

4. Crystallization Kinetics in the Presence of Coil-Crystalline Micelles

In the introduction, we mentioned that the action of coil-crystalline BCP micelles in suppressing precipitation of long alkane chains relies on the competition between two different kinetic processes: normal nucleation in the bath and nucleation onto the crystal core of the micelles. In this section we shall consider these processes in more detail as well as calculate the crystallization rate of long alkanes onto the crystal cores of micelles.

In normal nucleation in the bath, the rate of nucleation is controlled by two different energy barriers: the minimum work done $R_{\min}$ in creating a nucleus of critical size, and the energy barrier associated with diffusion across the bath/nucleus interface (the phase boundary) E_c [21,22], *i.e.*

$$\text{rate of crystallization } \propto \exp(-(R_{\min} + E_c)/k_B T).$$

Nucleating onto the pre-existing crystal core of a micelle on the other hand involves a lower energy barrier (only E_c) since the creation of a critical nucleus is no longer necessary. Introducing micelles with crystal cores into the mixed alkane bath therefore short circuits normal nucleation by providing a lower energy kinetic path for nucleation.

From crystallization experiments on pure n-alkanes with similar molecular weights as C_{36}, a value of $E_c/k_B T \sim 5.5$ is reported at the melting temperature, $T_m \approx 75$ °C [22,23]. If we assume that we have the same barrier height in the case of C_{36} crystallizing onto a lamellar crystal from a mixed alkane bath, at the crystallization temperature of dilute C_{36} in decane (~ -10 °C), we have $E_c/k_B T \sim 7.3$. Since the energy barrier for adsorbtion is very high, we will assume that the crystalization process is activation limited. This means that the hopping rate of molecules across the energy barrier is slow so that we can consider the distribution of solvent molecules adjacent to the phase boundary as being in thermodynamic equilibrium. In this case the current density (*i.e.* the number of long alkanes diffusing across the barrier per unit time per unit area) of crystallization onto the PE surface, J', is given by

$$J' = k_a \phi_2' \tag{20}$$

where k_a is the activation constant for crystallization and ϕ_2' is the concentration of long alkanes adjacent to the barrier in the liquid phase. Now ϕ_2' is just the thermodynamic concentration of long chains in the brush phase that we have calculated in the previous two sections, while k_a is given in terms of molecular parameters by [24]

$$k_a \approx \frac{D}{l} \exp\left(-\frac{E_c}{k_B T}\right). \tag{21}$$

Here D is the diffusion constant of the C_{36} chains in a bath of decane chains and l is the width of the adsorbtion barrier. The self diffusion constant of decane at -10 °C is $D_s = 6$ m^2/s [25]. Assuming Rouse type scaling for dilute C_{36} chains diffusing in a bath of decane, $D \approx D_s/4 = 1.5$ m^2/s. The width l has molecular dimensions, so we set $l \sim a \sim 8$ Å. Inserting these values and $E_c/k_B T \sim 7.3$ into equation (21), we arrive at the value $k_a \approx 10^6$ m/s for our system.

Since the suppression of long chain precipitation by coil-crystalline BCPs involves a competition between different kinetic processes, to optimise the action of the coil-crystalline BCPs, we need to maximize the rate of crystallization (*i.e.* no. of long alkanes crystallizing per unit time) onto the micellar cores; the BCP will be effective if this rate is greater than the rate of crystallization *via* normal nucleation in solution. To get the rate of crystallization onto the lamellar cores, we need to know the total area of micellar crystal cores in solution. We will make the simplifying assumption that most of the coil-crystalline BCPs are in large lamellar aggregates so that we can neglect the surface area of the "rims" of the lamellar crystals. In this case, the micellar core area per unit volume of solution is just $2c\Sigma$, where c is the number concentration of BCPs in solution and Σ is the interfacial area per brush given by equation (2) (the factor of 2 accounts for the top and bottom surface of the lamellar core, see Fig. 1). The specific rate of crystallization (*i.e.* rate per unit volume) onto the micellar cores r' is therefore given by

$$r' = 2c\Sigma J' = 2c\Sigma k_a \phi_2'. \tag{22}$$

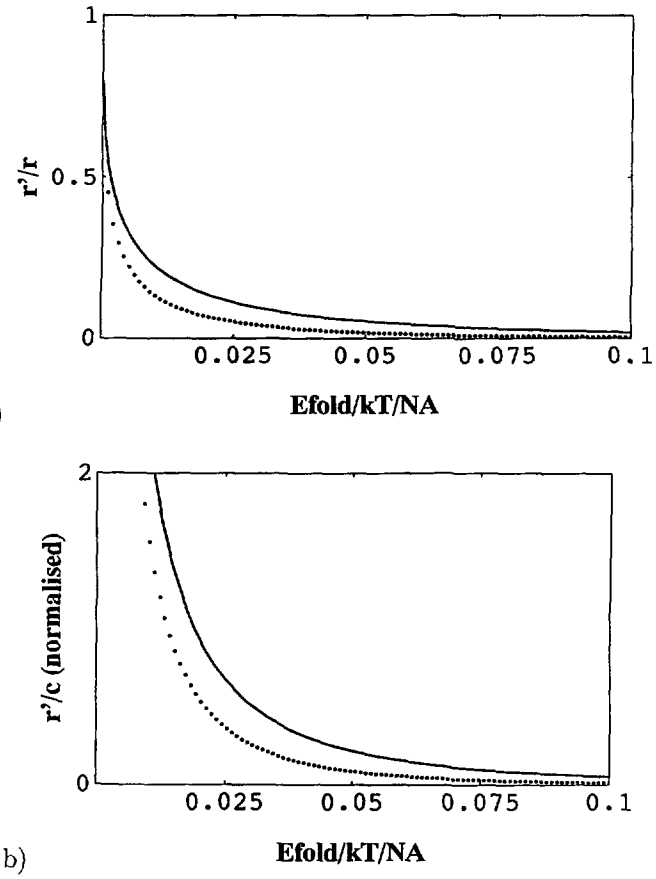

Fig. 6. — a) Relative specific rate of crystallization r'/r *vs.* $E_{\text{fold}}/N_{\text{A}}kT$ for $E_{\text{fold}}/kT = 7$, $N_1 = 2$, $N_2 = 8$, $\phi_1 = 0.98$, $\phi_2 = 0.02$ where r' and r are respectively the rates of crystallization in the presence and absence of the polymer brush layer. Solid line without nematic interaction ($\chi_{\text{n}} = 0$); dotted line for maximum nematic interaction ($\chi_{\text{n}} = 1$). b) Normalized rate of crystallization per chain $(r'/c)/(2a^2 k_{\text{a}}\phi_2)$ *vs.* $E_{\text{fold}}/N_{\text{A}}kT$ for $E_{\text{fold}}/kT = 7$, $N_1 = 2$, $N_2 = 8$, $\phi_1 = 0.98$, $\phi_2 = 0.02$; solid line without nematic interaction ($\chi_{\text{n}} = 0$); dotted line for maximum nematic interaction ($\chi_{\text{n}} = 1$).

The particularly simple scaling of r' with c in equation (22) means that if we know the specific rate for normal nucleation in solution, we can easily work out the concentration of BCP required to suppress crystallization *via* nucleation.

In Figure 6a, the relative rate of crystallization r'/r is plotted against $E_{\text{fold}}/kTN_{\text{A}}$, where r is the rate of crystallization onto the lamellar crystal core in the absence of the corona. From equation (22), $r = 2c\Sigma k_{\text{a}}\phi_2$, so that $r'/r \doteq \phi_2'/\phi_2$. The solid curve represents the flux in the absence of nematic interaction (*i.e.* $\chi_{\text{n}} = 0$), while the dotted line is the flux for maximum nematic interaction (*i.e.* $\chi_{\text{n}} = 1$). We have chosen the same parameters for the dotted line as for the solid line, *i.e.* $E_{\text{fold}}/kT = 7$, $N_1 = 2$, $N_2 = 8$, $\phi_1 = 0.98$, $\phi_2 = 0.02$. From Figure 6a, we see that r'/r is a monotonically decreasing function of $E_{\text{fold}}/kTN_{\text{A}}$. Also the flux onto the micellar core is always smaller than that onto a bare crystal surface ($r'/r < 1$) for all micellar parameters, showing that the presence of the brush layer above the lamellar crystal has a negative effect on the crystallization flux. In the limit $E_{\text{fold}}/kTN_{\text{A}} \to 0$ our

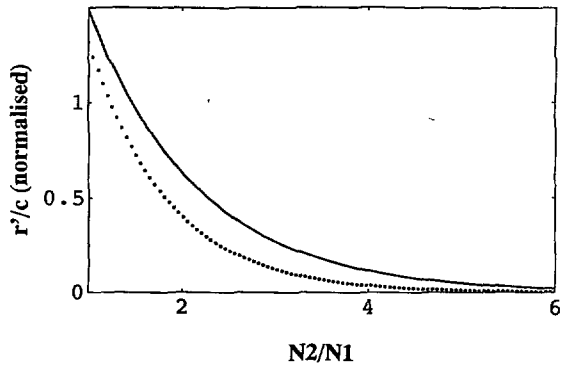

Fig. 7. — Normalized rate of crystallization per chain $(r'/c)/(2a^2k_a\phi_2)$ *vs.* N_2/N_1 for $E_{fold}/kT = 7$, $N_1 = 2$, $N_A = 100$, $\phi_1 = 0.98$, $\phi_2 = 0.02$; solid line without nematic interaction ($\chi_n = 0$); dotted line for maximum nematic interaction ($\chi_n = 1$).

calculation predicts that $r'/r \to 1$. As explained in Section 2, this is due to the entropic elasticity dominating over interfacial tension so that the solvent concentration in the corona approaches that of the bath. In the opposite limit of large E_{fold}/kTN_A, r'/r becomes very small. This obviously breaks down for the case of fixed E_{fold} since we do not recover the bare crystal limit ($r'/r \to 1$) for $N_A \to 0$. The reason for this is the strong stretching approximation (*i.e.* Alexander-de Gennes model) that we have used for the corona chains breaks down in this limit. Presumably, if we used a more accurate SCF treatment for the brush phase [10], we would recover the bare crystal core limit for $N_A \to 0$.

In Figure 6b, we plot the rate of crystallization per BCP chain r'/c (normalized by $2a^2k_a\phi_2$, *i.e.* $r'/(2ca^2k_a\phi_2) = (\phi_2'/\phi_2')(\Sigma/a^2)$) against E_{fold}/kTN_A for $\chi_n = 0$ (full line) and $\chi_n = 1$ (dotted line). The parameters are the same as for Figure 6a. We see that the rate of crystallization is a stong function of both core parameters (*i.e.* E_{fold}) and brush parameters (*i.e.* N_A, χ_n) of the coil-crystalline micelle. Also r'/c is maximum when E_{fold}/kTN_A is made as small as possible. This is due to a combination of two effects: firstly the solvent concentration in the brush phase approaching that of the bath (Fig. 6a); secondly, the area of the crystal core per brush chain available for crystallization is maximum for small E_{fold}/kTN_A (Fig. 3). For a specific BCP chemistry (*e.g.* PE-PEP), the only parameter in the system that can be varied is N_A; in this case, our calculation suggests that N_A should be made as large as possible to maximize r'. Although, strictly speaking, our theoretical calculation only applies in the long chain (*i.e.* strong stretch) brush limit (*i.e.* $h/R_g \gg 1$), whereas for the system of Richter *et al.*, the brush is in the intermediate stretch regime ($h/R_g \approx 3-5$), it is nonetheless instructive to compare our theoretical calculation with their experimental system. For their system, typically we have $E_{fold}/kTN_A = 0.07$. In this case, Figure 6b indicates that there is a lot of room for improvement from increasing the molecular weight of corona chains. One point worth mentioning here is that in the quest to improve the anti-precipitation performance of the coil-crystalline micelles, one might be tempted to go to the opposite limit of $N_A \to 0$ (*i.e.* the bare crystal limit). However by reducing the proportion of soluble blocks in the micelle, we run the risk of precipitating the whole micelle out of solution.

In Figure 7, we plot r'/c (normalised by $a^2k_a\phi_2$) against N_2/N_1. As before, the solid curve represents the flux in the absence of nematic interaction while the dotted line is the flux for maximum nematic interaction. The other system parameters are $E_{fold}/kT = 7$, $N_A = 100$, and

we set $N_1 = 2$, $\phi_1 = 0.98$, $\phi_2 = 0.02$. Clearly, the crystallization rate of the long alkane chain falls with increasing length relative to the short alkanes. This shows that the anti-precipitation action of the BCP is greatest in the case where the disparity in length between the long and short chains in the bath is small.

5. Conclusions

Motivated by recent experiments by Richter *et al.*, we have in this paper looked at the thermodynamics and kinetics of lamellar coil-crystalline BCP micelles in a bimodal solvent bath. Assuming an Alexander-de Gennes brush model for the strongly stretched corona chains and explicitly accounting for the polydispersity of the solvent chains, we have calculated the thermodynamic distribution of long to short solvent chains in the micellar corona. Both for zero and maximum nematic interactions in the corona phase ($\chi_n = 0$ and $\chi_n = 1$ respectively), we find that $\phi_2'/\phi_1' < \phi_2/\phi_1$ for all micellar parameters (*i.e.* short chains predominate in the corona compared to in the bath). Our calculation therefore shows that the swelling of the micellar corona by long alkane chains observed by Richter *et al.* is not a thermodynamic effect. This supports the suggestion that the micellar cores act as nucleation sites for long alkane chain crystallization.

By looking at the different crystallization mechanisms in detail, we propose that coil-crystalline BCP micelles suppress long alkane crystallization/precipitation at low temperatures by providing a lower kinetic route to crystallization compared to normal nucleation in the bath. Specifically nucleating onto the micellar crystal core involves a lower energy barrier compared to crystallizing normal nucleation (*i.e.* E_c instead of $E_c + R_{min}$). By assuming that the nucleation onto the lamellar micelle core is activation limited, we calculate the specific rate of this process and find that it scales linearly with c (the number concentration of BCPs) and is dependant on both core and corona parameters of the micelle. In particular, we predict that to maximize the crystallization rate per BCP, both E_{fold}/kTN_A and χ_n need to be made as small as possible. This leads us to the surprising conclusion that for a given BCP chemistry, increasing the molecular weight of the solvated block increases the rate of long solvent chain crystallization onto the micellar crystal core. We also find that the anti precipitation action of the coil-crystalline BCP is increases when the length of the long solvent chain is reduced relative to that of the short solvent chain.

Acknowledgments

We are grateful to our BRITE-EURAM project partners Dr. R.N. Young, Prof. N. Hadjichristidis for useful discussions and Dr. M. Prager, Dr. A. Ramzi and Prof. D. Richter for useful discussions and showing us their neutron scattering data. We would also like to thank Peter Olmsted for helpful suggestions and comments, Paul van der Schoot for pointing out how to deal with nematic order of flexible chains and Graeme Bishko for help with graphics. This project was carried out under the BRITE-EURAM project (project no. BE 5543) on the synthesis and characterisation of hetero-armed star block copolymers.

References

[1] Schneiders D., Ph.D. Thesis, University of Aachen, Germany, 1996.
[2] Monkenbusch M., Schneiders D., Richter D., Farago B., Fetters L. and Huang J., *Nuovo Cimento Della Societa Italiana di Fisica D* **16** (1994) 747.
[3] Monkenbusch M., Schneiders D., Richter D., Farago B., Fetters L. and Huang J., *Physica B* **213** (1995) 707.
[4] Denis J. and Durand J.P., *Revue de L'Institut Français du Petrole* **46** (1991) 637; Gerson A.R., Roberts K.J. and Sherwood J.N., *Powder Technology* **65** (1991) 243.
[5] Wittman J.C. and Lotz B., *J. Polym. Sci.: Polymer Physics Edition* **23** (1985) 205.
[6] Perček V. and Tsuda Y., *Macromol.* **23** (1990) 3509.
[7] Yurasova T.A. and McLeish T.C.B., *Polymer* **34** (1993) 3774.
[8] Alexander S., *J. Phys. France* **38** (1977) 983.
[9] de Gennes P.-G., *J. Phys. France* **37** (1976) 1443; de Gennes P.-G., *Macromol.* **13** (1980) 1069.
[10] Milner S.T., Witten T.A. and Cates M.E., *Macromol.* **21** (1988) 2610.
[11] Schmidt-Rohr K. and Spiess H.W., *Macromol.* **24** (1991) 5288.
[12] Vilgis T. and Halperin A., *Macromol.* **24** (1991) 2090.
[13] Sanchez I.C., *Encycl. Polym. Sci. Technol.* **11** (1987) 1.
[14] Khokhlov A.R. and Semenov A.N., *Physica* **108A** (1981) 546.
[15] Khokhlov A.R. and Semenov A.N., *Physica* **112A** (1982) 605.
[16] Odijk T., *Macromol.* **19** (1986) 2313.
[17] Onsager L., *Ann. N.Y. Acad. Sci.* **51** (1949) 627
[18] Hentschke R., *Macromol.* **23** (1990) 1192.
[19] Brereton M.G. and Ries M.E., *Macromol.* **29** (1996) 2644.
[20] Olmsted P.D. and Milner S.T., *Macromol.* **27** (1994) 6649.
[21] Turnbull D. and Fisher J.C., *J. Chem. Phys.* **17** (1949) 71.
[22] Hammami A., Mehrotra A.K., *Thermochimica Acta* **211** (1992) 137.
[23] Oliver M.J. and Calvert P.D., *J.Crystal Growth* **30** (1975) 343.
[24] Ma S.K., Statistical Mechanics (World Scientific, Singapore, 1985) p. 371.
[25] Douglass D.C. and McCall D.W., *J. Phys. Chem.* **100** (1996) 2661.